A projection of permafrost degradation on the Tibetan Plateau during the 21st century

Donglin Guo,[1,3] Huijun Wang,[1,2] and Duo Li[4]

Received 11 July 2011; revised 30 December 2011; accepted 30 December 2011; published 3 March 2012.

[1] The current distribution and future change of permafrost on the Tibetan Plateau were examined using the Community Land Model version 4 (CLM4) with explicit treatment of frozen soil processes. When forced off-line with archived high-resolution data from The Abdus Salam International Centre for Theoretical Physics Regional Climate Model version 3 nested within the Model for Interdisciplinary Research on Climate 3.2 HiRes, the CLM4 produced a near-surface permafrost area of 122.2×10^4 km^2 for the Tibetan Plateau. This area compares reasonably with area estimates of 126.7×10^4 km^2 for the Plateau frozen soil map. In response to the simulated strong Plateau warming (approximately 0.58°C per decade over the Tibetan Plateau for the period from 1980 to 2100 under the A1B greenhouse gas emissions scenario), the near-surface permafrost area is projected to decrease by approximately 39% by the mid-21st century and by approximately 81% by the end of the 21st century. The near-surface permafrost area exhibits a significant decreasing linear trend, with a rate of decrease of 9.9×10^4 km^2 per decade. The simulated deep permafrost area remains longer than the near-surface permafrost for the same period. The active layer thickness of 0.5–1.5 m found in the present-day increases to approximately 1.5–2.0 m by the period of 2030–2050. This increase will continue and reach a level of 2.0–3.5 m by the period of 2080–2100. Surface runoff decreases but subsurface runoff increases, both relative to the difference between precipitation and evapotranspiration. This is related to the fact that the decrease in ground ice content, as caused by permafrost degradation, facilitates the percolation of more water to deeper soil layers, thus resulting in the reallocation of runoff. These results provide useful references for evaluating the level of permafrost degradation in response to climate warming on the Tibetan Plateau.

Citation: Guo, D., H. Wang, and D. Li (2012), A projection of permafrost degradation on the Tibetan Plateau during the 21st century, *J. Geophys. Res.*, *117*, D05106, doi:10.1029/2011JD016545.

1. Introduction

[2] The global climate has become warmer over the last century and is projected to undergo further warming in the next 100 years [e.g., *Jones and Briffa*, 1992; *Meehl et al.*, 2007]. The warming has not been globally uniform; higher northern latitudes and high-altitude areas seem to be especially susceptible and vulnerable to climate change [*Houghton et al.*, 1996; *Messerli and Ives*, 1997; *Wang and Sun*, 2009]. Permafrost is defined as ground that remains at or below 0°C continuously for two or more years [*Muller*, 1947]. It is widespread in high latitudes and in high-elevation regions and is estimated to occupy approximately a quarter of the terrestrial Northern Hemisphere [*Brown et al.*, 1997; *Zhang et al.*, 1999; *Zhang et al.*, 2007]. As defined by ground temperature, permafrost is essentially a climatic phenomenon and is therefore potentially sensitive to climate change [*Anisimov et al.*, 2001]. An increase in air temperature can warm the ground through energy exchange at the surface and induce permafrost thaw. In turn, permafrost degradation, induced by climate warming, not only affects local hydrology, ecosystems, soil biogeochemistry, and engineering infrastructures [*Nelson et al.*, 2001; *Nelson*, 2003], but also may intensify climate warming through the release of organic carbon sequestered in permafrost [*Zimov et al.*, 2006; *Schuur et al.*, 2009].

[3] The implications of permafrost degradation in response to climate warming have drawn considerable attention in recent decades. Some studies associated with permafrost monitoring and simulation as well as projection of permafrost degradation have been reported [e.g., *Anisimov and Nelson*, 1997; *Stendel and Christensen*, 2002; *Nelson*, 2003; *Frauenfeld et al.*, 2004; *Lawrence and Slater*, 2005; *Delisle*, 2007; *Oelke and Zhang*, 2007; *Zhang et al.*, 2007,

[1]Nansen-Zhu International Research Center, Institute of Atmospheric Physics, Chinese Academy of Sciences, Beijing, China.
[2]Climate Change Research Center, Chinese Academy of Sciences, Beijing, China.
[3]Graduate University, Chinese Academy of Sciences, Beijing, China.
[4]National Climate Center, China Meteorological Administration, Beijing, China.

0148-0227/12/2011JD016545

2008; *Wu and Zhang*, 2008, 2010; *Yang et al.*, 2010]. International projects to explore the nature of permafrost were also conducted. For example, to characterize the thermal state of permafrost (TSP), the International Polar Year Project 50-TSP was launched by the International Permafrost Association. Also, the Circumpolar Active Layer Monitoring Program was designed to observe temporal and spatial variabilities of the active layer and its response to changes in climate conditions.

[4] The elevation of the Tibetan Plateau averages more than 4000 m and is nicknamed the "third pole" of the Earth; it is well known for its profound influences on both regional and global climates through thermal and dynamical forcings [e.g., *Ye and Gao*, 1979; *Manabe and Broccoli*, 1990; *Yanai et al.*, 1992; *Yanai and Wu*, 2006]. A large portion of the Plateau has experienced marked climate warming (an average increase of 0.28°C per decade) since the early 1960s [*Guo and Wang*, 2012]. Moreover, a warming of 0.28°C–0.61°C will could occur over the Tibetan Plateau during the next 100 years according to the Intergovernmental Panel on Climate Change (IPCC) Fourth Assessment Report (IPCC AR4) under the Special Report on Emissions Scenarios (SRES) A1B (a "middle-of-the-road" estimate of future emissions) scenario [*Meehl et al.*, 2007]. This significant warming is likely to result in the degradation of permafrost on the Tibetan Plateau.

[5] A significant portion of the Tibetan Plateau is underlain by permafrost. Seasonal freezing and thawing processes in the surface layers, along with their spatial distribution, result in time-space variations of surface wetness and variations in the surface heat balance. Such variations strongly affect the Plateau's seasonal transitions [*Yang et al.*, 2003], surface energy flux variations [*Guo et al.*, 2011a, 2011b], and atmospheric circulation over East Asia [*Wang et al.*, 2003], thus having profound implications for subsequent monsoon behavior and global climate processes [*Barnett et al.*, 1989; *Vernekar et al.*, 1995; *Su et al.*, 2006]. Additionally, the Qinghai-Tibet railway traverses the Tibetan Plateau from north to south, stretching across a distance of 1118 km. Approximately 550 km of the railway is underlain by permafrost [*Cheng*, 2002]. The population in the Tibetan Plateau region has also tripled over the last 45 years and is likely to continue to grow, which will be accompanied by accelerated industrial and urban development [*Fu and Zheng*, 2000]. Both the scientific implications, such as the impact on the regional ecosystem and climate change, and the economic value, such as the construction and maintenance of human infrastructures, require a detailed investigation and a projection of the permafrost degradation that could result from climate warming.

[6] Based on in situ measurements from monitoring boreholes along the Qinghai-Tibet Highway, recent studies indicate that mean annual permafrost temperatures at a depth of 6.0 m have increased by 0.12°C–0.67°C during the period from 1996 to 2006, with an average increase of 0.43°C [*Wu and Zhang*, 2008]. The active layer has increased by 7.5 cm per year from 1995 to 2007 [*Wu and Zhang*, 2010]. An increase of 25 and 50–80 m in lower altitudinal limits of permafrost occurred in the north during the last 30 years and in the south over the last 20 years, respectively [*Cheng and Wu*, 2007]. However, field observational sites are sparse on the Plateau, meaning that few studies have focused on the regional scale and on long-term changes in permafrost in response to climate warming.

[7] Using climatic forcing from the Hadley Centre Coupled Model version 2 (HadCM2) scenario of climate change, *Li and Cheng* [1999] applied a geographic information system- (GIS-) aided altitude model to project future permafrost distributions on the Tibetan Plateau. By considering an air temperature increase of 0.2°C or 0.52°C per decade, *Nan et al.* [2005] employed a mean annual ground temperature model to provide insight into future permafrost dynamics on the Tibetan Plateau. However, these previous works used statistical-empirical models as well as some simple assumptions. Few works have focused on the simulation of permafrost on the Tibetan Plateau using numerical models. *Lawrence and Slater* [2005] used the fully coupled Community Climate System Model version 3 (CCSM3) to examine transient near-surface permafrost evolution north of 45°N during the 21st century. Their results generated significant discussion for reasons largely related to the shallow soil profile and the importance of the organic layer of the surface [*Burn and Nelson*, 2006; *Lawrence and Slater*, 2006; *Delisle*, 2007; *Yi et al.*, 2007]. Subsequent works focused on the development of land-surface models for the soil temperature simulation and a series of other improvements and addition of new capabilities, which promoted the release of the Community Land Model version 4 (CLM4) [*Lawrence et al.*, 2011].

[8] In this study, we investigated the current distribution and future change of permafrost on the Tibetan Plateau using the CLM4, which is forced off-line with archived high-resolution data from The Abdus Salam International Centre for Theoretical Physics Regional Climate Model version 3 nested within the Model for Interdisciplinary Research on Climate 3.2 HiRes. In section 2, a brief description of the model, experimental design, and methods is provided. In section 3, we provide the simulated results and analyze the impact of permafrost degradation on local hydrological processes. A comparison with previous research results and discussions of plausibility of this projection and potential sources of possible uncertainty in the projections of permafrost degradation are provided in section 4, while a summary is presented in section 5.

2. Model, Experimental Design, and Methods

2.1. General Circulation Model

[9] The general circulation model (GCM) used herein is the coupled Model for Interdisciplinary Research on Climate 3.2 HiRes (MIROC3.2 HiRes), which was developed cooperatively by the Center for Climate System Research (CCSR), National Institute for Environmental Studies (NIES), and Frontier Research Center for Global Change (FRCGC) of Japan [*Hasumi and Emori*, 2004]. The model consists of five component models: the atmosphere, land surface, ocean, sea ice, and river, coupled by a flux coupler. The atmospheric model solves the primitive equations on a sphere using a spectral transform method. The horizontal resolution is approximately 1.125° × 1.125° in longitude and latitude. The height of the model top is approximately 40 km. The model has 56 vertical σ layers with relatively finer vertical resolution in the planetary layer and around the tropopause. The cloud parameterization scheme was

represented using the large-scale precipitation scheme of *Le Treut and Li* [1991], in which the second indirect effect of aerosols was considered. The convection parameterization scheme employed the closure assumption scheme of *Arakawa and Schubert* [1974], based on the scheme of *Pan and Randall* [1998], and added to by an empirical suppression condition introduced by *Emori et al.* [2001]. The boundary layer scheme used the level 2 scheme of turbulence closure of *Mellor and Yamada* [1982]. The radiative transfer scheme employed is based on the two-stream discrete ordinate method and the k distribution method. The horizontal resolution of the land-surface model is approximately 0.5625° × 0.5625° in longitude and latitude. The surface processes were carried out with the minimal advanced treatments of surface interaction and runoff, which is described by *Takata et al.* [2003]. The surface fluxes over snow-free and snow-covered areas are calculated separately and averaged afterward, weighted with area fractions. The model has one canopy layer, five soil layers, and a variable number (0–3) of snow layers. The total thickness of the soil layer is 2 m. The freezing (thawing) of soil water is calculated when the soil temperature is below (above) the freezing point and the unfrozen soil moisture is higher (lower) than zero. The ocean model has 47 vertical levels, and the vertical coordinate is a hybrid of σ and z. The horizontal resolution of the ocean model is approximately 0.28125° × 0.1875° in longitude and latitude. The horizontal resolution of the sea ice model is considered to be the same as that of the ocean model. More detailed information of the MIROC3.2 HiRes can be found in the document of *Hasumi and Emori* [2004]. The simulation during the period from 1948 to 2100 was selected to drive the regional climate model (RegCM3). The simulation used observed greenhouse gases concentrations for the present-day simulation of 1948–2000 and greenhouse gases forcing from the IPCC A1B emission scenario for the future period of 2001–2100 [*Intergovernmental Panel on Climate Change*, 2000].

[10] Among the 22 GCMs participating in the Coupled Model Intercomparison Project phase 3 experiment, MIROC3.2 HiRes was one of the models that produced the most reasonable mean climate states for the regions in East Asia [*Xu et al.*, 2007]. For the annual mean air temperature and precipitation, the spatial correlation coefficients between the simulated results and observations were 0.96 and 0.80, respectively [*Xu et al.*, 2007]. Previous analysis also showed its good performances in simulating Northern Hemisphere winter midlatitude atmospheric variability [*Lucarini et al.*, 2007]. In addition, the MIROC3.2 HiRes has high spatial resolution (T106, approximately 125 km) and provides 6 hourly output data, which is appropriate to drive the high-resolution regional simulation at a 25 km grid spacing. Therefore, we chose MIROC3.2 HiRes to drive the regional climate model.

2.2. Regional Climate Model

[11] The regional climate model employed in this study is the Abdus Salam International Centre for Theoretical Physics Regional Climate Model version 3 (RegCM3) [*Pal et al.*, 2007]. The RegCM3 was validated to be applicable for the simulation of the climate over China and East Asia and has been used in a wide variety of applications during the past decade [*Gao et al.*, 2001, 2006, 2008; *Ju et al.*, 2007; *Gao and Giorgi*, 2008; *Shi et al.*, 2009, 2011].

[12] The model has 18 vertical layers up to a 10 hPa top. The atmospheric radiation transfer was computed using the radiation package from the National Center for Atmospheric Research (NCAR) Community Climate Model version 3 (CCM3). The ocean flux parameterization followed the work by *Zeng et al.* [1998]. The planetary boundary layer computations employed the nonlocal formulation of *Holtslag et al.* [1990]. Convective precipitation was represented using the scheme of *Grell* [1993], based on the closure assumption of *Fritsch and Chappell* [1980], while large-scale precipitation was represented using the Subgrid Explicit Moisture Scheme. The land surface processes were accomplished with the Biosphere-Atmosphere Transfer Scheme (BATS) [*Dickinson et al.*, 1993]. The BATS has a vegetation layer, a snow layer, a surface soil layer, 10 cm thick, or root zone layer, 1–2 m thick, and a third deep soil layer 3 m thick. The freezing and melting processes are considered to occur in a range between the freezing-point temperature and some temperature below the freezing-point temperature. The model vegetation cover is obtained from the observed data by *Liu et al.* [2003] within the Chinese territory and from the satellite based on the Global Land Cover Characteristics (GLCC) database outside China.

[13] The lateral buffer zone included 24 grid point rows. The horizontal resolution of the model was 25 km, and the simulation domain covered all of China and the surrounding areas of East Asia, with the center at 35°N, 109°E, and the 288 × 219 (east-west by north-south) grid points. The initial and time-evolving lateral boundary conditions were provided by the MIROC3.2 HiRes simulation.

2.3. CLM4

[14] The land-surface model used in this study is the CLM4 [*Oleson et al.*, 2010], which can be run as a component of the Community Climate System Model version 4. CLM4 is the upgrade from the previous version, CLM3.5. The released version of CLM3 suffers from deficiencies in the simulations of the hydrological cycle. These deficiencies have been eliminated largely through a series of modifications to the CLM3, which includes revised surface data sets based on Moderate Resolution Imaging Spectroradiometer (MODIS) data [*Lawrence and Chase*, 2007], reductions in canopy interception [*Lawrence et al.*, 2007], incorporation of a two-leaf model for photosynthesis [*Thornton and Zimmerman*, 2007], new parameterizations for frozen soil, soil water availability, and soil evaporation, a TOPMODEL-based model for surface and subsurface runoff, and a groundwater model for determining water table depth [*Niu et al.*, 2007]. Changes to CLM4 beyond CLM3.5 include a modification to with a revised numerical solution of the Richards equation [*Zeng and Decker*, 2009; *Decker and Zeng*, 2009]; the snow model is significantly modified via incorporations of snow and ice aerosol radiation, a new density-dependent snow cover fraction parameterization, and a revised snow burial fraction over short vegetation and corrections to snow compaction [*Flanner et al.*, 2007; *Niu and Yang*, 2007; *Wang and Zeng*, 2009; *Lawrence and Slater*, 2010]; the model is extended with a carbon-nitrogen biogeochemical model [*Thornton et al.*, 2007, 2009]; and the model includes a representation of organic soil and deep soil

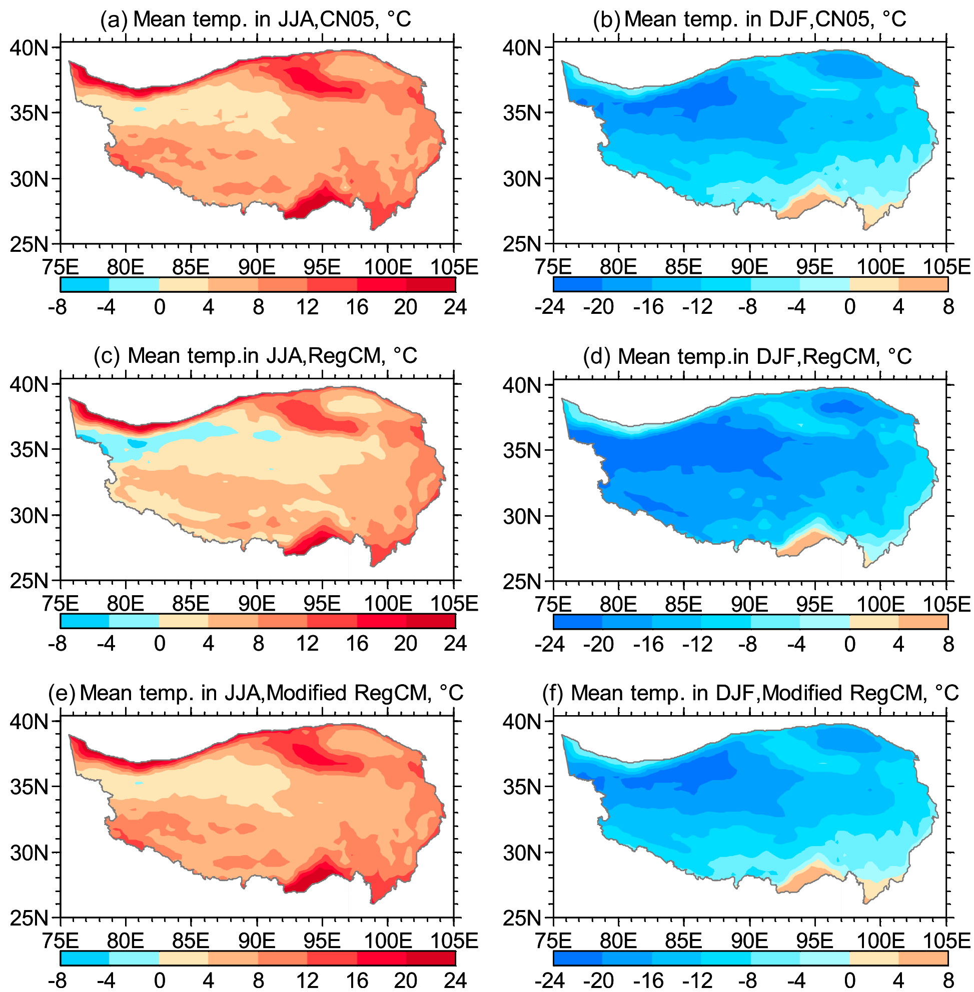

Figure 1. Mean air temperature of the forcing data set that is averaged for the period from 1981 to 2000. Mean air temperatures from (a) the CN05, (c) the RegCM3, and (e) the modified RegCM in the summer (JJA). Mean air temperatures from (b) the CN05, (d) the RegCM3, and (f) the modified RegCM in the winter (DJF).

into the existing mineral soil treatment to enable a more realistic modeling of permafrost [*Lawrence and Slater*, 2008; *Lawrence et al.*, 2008].

[15] In CLM4, the frozen soil processes obtain an explicit treatment. The temperature profile is calculated by numerically solving the second law of heat conduction equation first without phase change. Then, soil temperatures are evaluated to determine whether a phase change should take place. If the new soil temperatures indicate that a phase change has taken place, the excess or deficit of energy is determined and used to melt or freeze the soil water and the temperatures are adjusted back to the freezing level [*Oleson et al.*, 2010]. The freezing and melting processes are updated by means of the incorporation of a freezing-point depression expression that permits liquid water to coexist with ice over a wide range of temperatures below 0°C and that enhances permeability into partially ice-filled soil [*Niu and Yang*, 2006]. The model represents the thermal and hydraulic properties of soil organic matter, which produces reductions in soil temperature and permits incident precipitation to quickly permeate through the topsoil layers [*Nicolsky et al.*, 2007; *Lawrence and Slater*, 2008]. The ground column has been extended to approximately 50 m depth, making a total of 15 ground layers. Layer thicknesses exponentially increase with depth. The upper 10 layers are hydrologically active while the bottom 5 layers are thermal slabs that are not hydrologically active. The deepening of the soil column can contribute to account for the thermal inertia provided by the cold deep permafrost layers [*Nicolsky et al.*, 2007; *Alexeev et al.*, 2007; *Lawrence et al.*, 2008].

2.4. Experimental Design

[16] The regional simulation was conducted for the period from 1 January 1948 to 31 December 2100. The first 3 years were used as the period of initialization for the RegCM3. The RegCM3 is forced with the MIROC3.2 HiRes boundary forcing. *Shi* [2010] presented a validation of the ability of this regional simulation to simulate the present climate over China through a comparison between the simulated results and observations. For air temperature and precipitation, the spatial correlation coefficients between the simulation and the observations were 0.976 and 0.813, respectively.

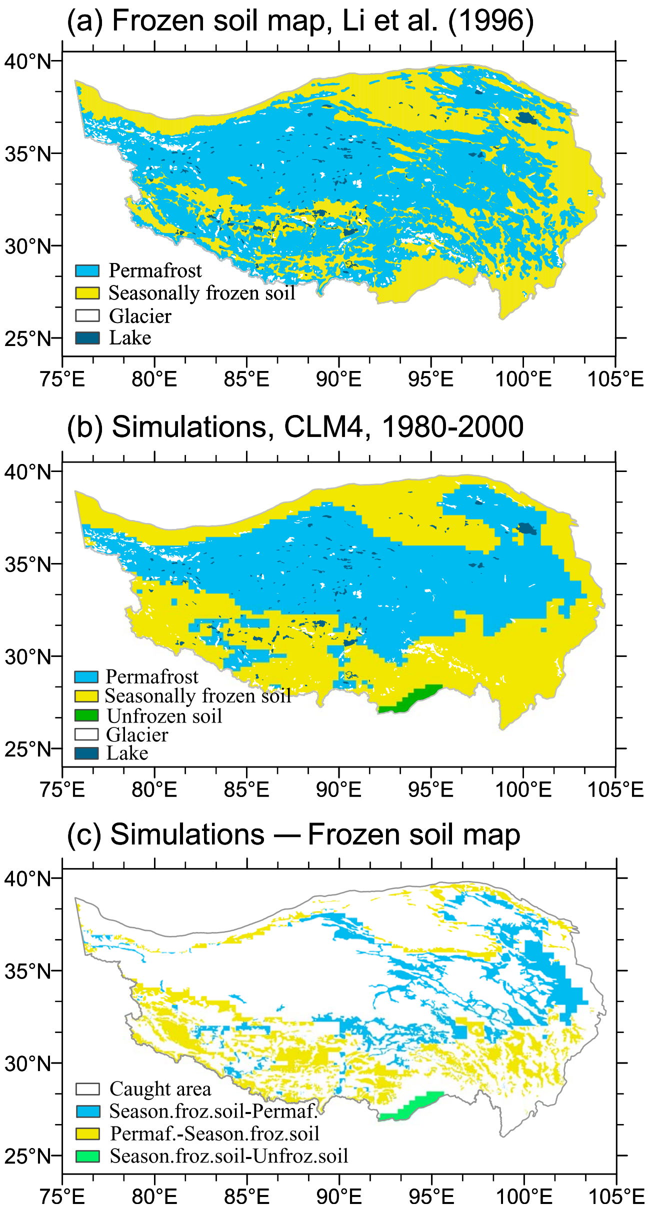

Figure 2. (a) The frozen soil map [after the work by *Li and Cheng*, 1996], (b) the simulated frozen soil area that is averaged over the period from 1980 to 2000, and (c) the difference map between the simulated frozen soil area and the frozen soil map. In the difference map of 2c, white refers to the area caught by the CLM4, blue refers to the area in which seasonal frozen soil was simulated into permafrost, yellow refers to the area in which permafrost was simulated into seasonal frozen soil, and green refers to the area in which seasonal frozen soil was simulated into unfrozen soil.

Here, we validate the performance of RegCM3 to simulate the air temperature on the Tibetan Plateau by assessing the level of agreement between the observations and the simulation because air temperature is a climatic factor closely related to permafrost. The temperature data used for this model validation were the daily temperature grid data from the China Meteorological Administration (CN05) at a 0.5° × 0.5° resolution. These data were constructed from an interpolation of 751 observation stations in China over the period from 1961 to 2005 [*Xu et al.*, 2009].

[17] As shown in Figure 1, when nested within the MIROC3.2 HiRes, the RegCM3 was able to accurately reproduce the spatial distribution features of the observed air temperatures on the Tibetan Plateau; however, the model simulated a systematically lower air temperature than the temperatures observed empirically in the summer and the winter. The spatial correlation coefficients between the simulations and observations were 0.90 in winter and 0.92 in summer, with mean biases of −3.2°C and −2.3°C, respectively. A correction to the systematic biases of the simulated results was performed using the method presented in section 2.5. After correction, the simulated temperatures fit closely with the observed results (Figure 1). The spatial correlation coefficients between the simulations and observations were almost 1.0 in both the winter and the summer, with mean biases of 0.01°C in both seasons.

[18] The atmospheric forcing elements required by CLM4 include 6 hourly radiation flux, precipitation, wind speed, air temperature, specific humidity, and atmospheric pressure. Air temperature was taken from the corrected results, and the other elements were directly provided by RegCM3. We performed a regional simulation with CLM4 and selected CLM_QIAN as the DATM mode. The horizontal resolution of the simulation was 0.31° × 0.23° in longitude and latitude, and the model domain ranged from 20°N to 45°N and from 70°E to 105°E. The simulations were spun up for 400 years with data from 1951. Soil temperature trends at all soil levels were below 0.001°C per year by the end of the spin-up phase. The transient simulation was conducted for the period from January 1951 to December 2100.

2.5. Methods

[19] The near-surface permafrost extent is defined as the integrated area where monthly mean soil temperatures in at least one soil level in the top 4.7 m of soil remained below 0°C for 24 consecutive months. The difference from the definition of *Lawrence and Slater* [2005] is that we used the top 4.7 m rather than the top 3.5 m because the active layer thickness can reach 4.57 m for the Tibetan Plateau, according to the records of *Wu and Zhang* [2010]. Deep permafrost is defined, as shown by *Lawrence et al.* [2008], as perennially frozen ground at depths between 10 and 30 m. Seasonally frozen soil is defined as the integrated area where there is no soil level in the top 4.7 m of soil in which the monthly mean soil temperature remains below 0°C for 24 consecutive months but where there is at least one soil level in the top 4.7 m of soil in which the monthly mean soil temperature remains below 0°C for a period of 24 consecutive months. Unfrozen soil is defined as the integrated area where monthly mean soil temperatures in all soil levels of the top 4.7 m of soil remain above 0°C for 24 consecutive months. Active layer thickness is defined as the depth of the deepest soil level that thaws at some point during the 24 consecutive months.

[20] Systematic biases of simulated air temperature were corrected in the following way: For each year during the period from 1971 to 2008, the temperature was adjusted by adding the difference between the observed mean and the simulated values that were averaged for the 10 years before the studied year; for each year during the period of

Table 1. Simulated Total Area Containing Frozen Soil (Excluding Glaciers and Lakes) ($\times 10^4$ km^2), for Selected Periods[a]

Types	1980–2000	2030–2050	2080–2100
Near-surface permafrost	122.2	74.9 (−39%)	22.9 (−81%)
Seasonally frozen soil	127.9	165.8 (+30%)	201.0 (+57%)
Unfrozen soil	1.2	10.3 (+758%)	27.3 (+2175%)

[a]Figures in the parentheses represent the relative change rates in percentages compared with the present-day (1980–2000) rates: "−" represents decrease, "+" represents increase.

1951–1970 and the period of 2009–2100, the temperature was adjusted by adding the difference between the observed mean and the simulated values that were averaged for 1999–2008. When we calculated the area of frozen soil, the Albers equal-area projection was applied to ensure that no area distortion occurred.

3. Results

3.1. Frozen Soil in CLM4

[21] The present-day (the mean from 1980 to 2000) frozen soil (including permafrost and seasonally frozen soil) area, as simulated by CLM4, is shown in Figure 2b. The present-day CLM4 permafrost area was qualitatively compared with the frozen soil map of the Tibetan Plateau (Figure 2a). This frozen soil map was produced by *Li and Cheng* [1996] based on observational borehole data and terrain data, which is currently thought to be the most reasonable map presenting the distribution features of frozen soil on the Tibetan Plateau [*Zhao*, 2004; *Wu*, 2005; *Cheng and Wu*, 2007]. As shown in Figure 2, the simulated permafrost distribution largely corresponds to the frozen soil map; however, the model cannot capture the detailed information (i.e., small and isolated permafrost areas). Specifically, CLM4 simulation converted some seasonally frozen soil into permafrost in the eastern Tibetan Plateau and converted some small-area and isolated permafrost into seasonally frozen soil in the southern Tibetan Plateau (Figure 2c). These disagreements between the simulated results and the frozen soil map could be partly attributed to the relatively large size of its grid boxes. Additionally, errors in other forcing data, e.g., precipitation (snowfall) and radiation, and inaccuracies in the surface and soil texture data sets could contribute to these disagreements though air temperature is corrected.

[22] The simulated permafrost covers a total of 122.2 $\times$ 10^4 km^2 (excluding glaciers and lakes), which compares favorably to the estimates of 126.7 $\times$ 10^4 km^2 of the frozen soil map, with a relative error of 3.5% (Table 1). Simulated seasonally frozen soil covers a total of 127.9 $\times$ 10^4 km^2 (excluding glaciers and lakes), which also compares favorably to the estimates of 122.4 $\times$ 10^4 km^2 of the frozen soil map, with a relative error of 4.5% (Table 1). The model yielded an area of unfrozen soil of 1.2 $\times$ 10^4 km^2, which is not present in the frozen soil map. It is seasonal frozen soil in the corresponding area of the frozen soil map.

[23] Permafrost temperature is one of the key variables for evaluation of permafrost simulation. *Wu and Zhang* [2008] presented the change in permafrost temperature from 1996 to 2006 using their data set from 10 boreholes. The simulated soil temperature was roughly compared with their results. Notably, the simulated soil temperature is a grid-mean value. In addition, the model did not directly calculate soil temperature at depths of 1 and 6 m. Soil temperatures at these two layers were estimated using a simple linear interpolation between the known values. For all 10 sites over the period of their own records, the observed mean soil temperatures at depths of 1 and 6 m ranged between −3.33°C and 0.34°C and between −3.43°C and −0.19°C, respectively, while the simulated soil temperature of the corresponding grids (i.e., the grids containing measured sites) at depths of 1 m and 6 m ranged between −6.83°C and −1.58°C and between −6.92°C and −1.81°C, respectively. In order to compare the changes in soil temperatures, the sites with observation periods of fewer than 8 years were eliminated because of their short records. The sites with negative increasing rates of soil temperatures were also eliminated as in the work of *Wu and Zhang* [2008]. For the remaining 4 sites, the observed increases in soil temperatures at depths of 1 and 6 m ranged between 0.13°C and 1.0°C and between 0.09°C and 0.67°C, respectively, over the period of their own records, while the simulated increases in soil temperatures at depths of 1 and 6 m ranged between 0.26°C and 0.58°C and between 0.23°C and 0.42°C, respectively, over the period of their own records. This comparison shows that the simulated soil temperatures are lower than those observed, and the simulated increases in soil temperatures are close to those of the observed results. A spatial mismatch exists because this comparison is based on grid-mean simulations and individual site observations. Especially, the observation sites are located in plains, basins, and valleys in relatively lower-altitude areas where the permafrost may be relatively warm [*Wu et al.*, 2010]. Despite the shortcomings of this comparison, the simulated soil temperatures could be basically reasonable.

[24] The simulated active layer thickness was also compared with data from a systematic soil temperature measurement network of 10 sites that monitored active layer thickness along the Qinghai-Tibetan Highway over the period from 1995 to 2007 [*Wu and Zhang*, 2010]. Measured active layer thicknesses along the Qinghai-Tibetan Highway typically ranged between 1.32 and 4.57 m, while the simulated active layer thicknesses of the corresponding grids ranged between 1.32 and 2.87 m. The simulated results are reasonable when we consider that the simulated active layer thickness is a value of the gridded area mean.

3.2. Degradation in Permafrost

[25] Projections of the permafrost area under the A1B emission scenario are shown in Figures 3a and 3b. Compared with the area averaged for the period from 1980 to 2000, mean near-surface permafrost areas clearly decrease by the years 2030–2050. This decrease is reflected in that the permafrost at the edge is converted into seasonally frozen soil. A small area of permafrost in the southwestern Tibetan Plateau is also converted into seasonally frozen soil. This degradation occurs primarily at the southern and eastern edges of the simulated permafrost boundary. The near-surface permafrost area decreases from a mean of 122.2 $\times$ 10^4 km^2 for 1980–2000 to a mean of 74.9 $\times$ 10^4 km^2 for 2030–2050, with a relative decrease of 39% (Table 1). In contrast, the seasonally frozen soil area increases from a mean of 127.9 $\times$ 10^4 km^2 for 1980–2000 to a mean of 165.8 $\times$ 10^4 km^2 for 2030–2050, with a relative increase of

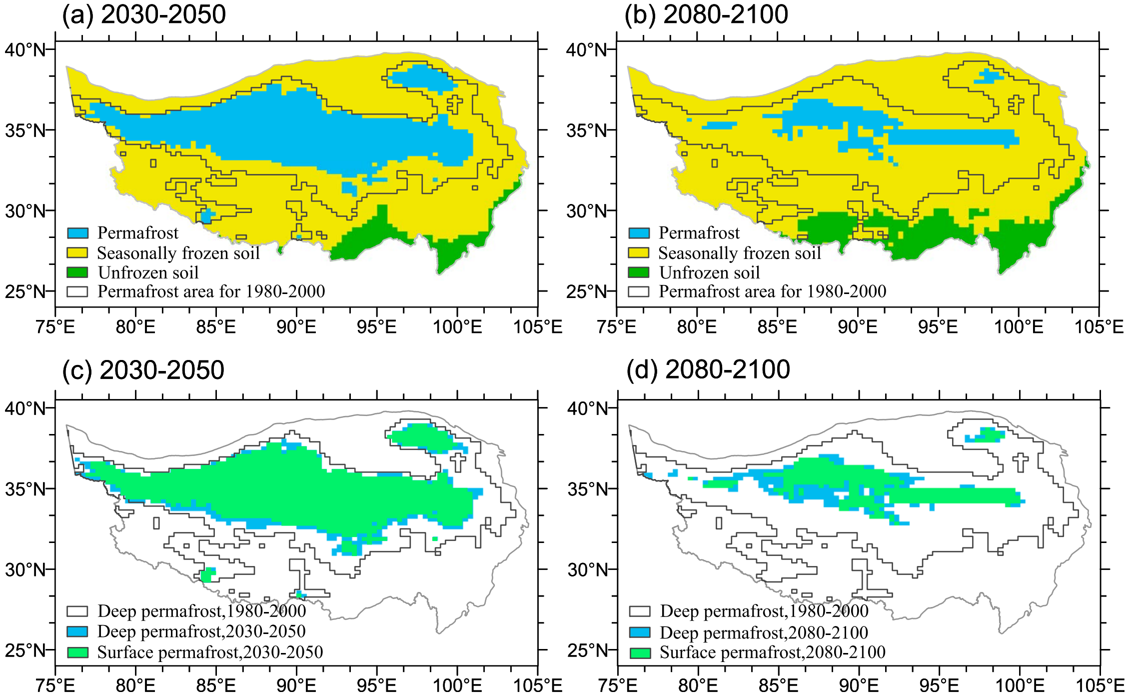

Figure 3. Mean near-surface permafrost areas, as simulated in the CLM4, averaged for the period of (a) 2030–2050 and (b) 2080–2100, as well as the simulated areas of deep permafrost averaged over the periods of (c) 2030–2050 and (d) 2080–2100. Deep permafrost is defined here as perennially frozen soil at depths between 10 and 30 m.

30% (Table 1). The unfrozen soil area in the southern edge of the Tibetan Plateau was also found to increase from a mean of 1.2 × 10^4 km^2 for 1980–2000 to a mean of 10.3 × 10^4 km^2 for 2030–2050. By the period of 2080–2100, only a 22.9 × 10^4 km^2 area of near-surface permafrost remains under the A1B emission scenario, which represents a decrease of 81% compared with the area during the period of 1980–2000 (Table 1). Meanwhile, the seasonally frozen soil area and unfrozen soil area extend farther, to 201.0 × 10^4 km^2 and 27.3 × 10^4 km^2, respectively.

[26] It should be stressed that much of the simulated near-surface permafrost degradation does not mean that all permafrost disappears. In CLM4, each grid box occupies an area of 0.31° × 0.23° in longitude and latitude and is represented by a single soil column, which means that some sporadic and isolated permafrost cannot be explicitly detected by the model. The simulated extents of deep permafrost as averaged for the periods of 2030–2050 and 2080–2100 are given in Figures 3c and 3d, respectively; deep permafrost is considered to indicate permafrost that is found between depths of 10 and 30 m. The simulated deep permafrost will degrade largely by the years 2030–2050 and by the years 2080–2100, compared with the period from 1980 to 2000. However, the mean deep permafrost area remains at an area of 89.8 × 10^4 km^2 for 2030–2050, which is larger than the 74.9 × 10^4 km^2 area of near-surface permafrost during this same period. Similarly, the mean deep permafrost remains at 35.2 × 10^4 km^2 during the period from 2030 to 2050, which is larger than the 22.9 × 10^4 km^2 area of near-surface permafrost during this same period. This indicates that there are some areas where, for a certain period, the simulated near-surface permafrost may disappear while the deep permafrost still exists.

[27] A time series of simulated near-surface permafrost areas is shown in Figure 4a. The simulated near-surface permafrost exhibits a significant decrease in the linear trend ($y = -0.99x + 169.48$, $R^2 = 0.99$, unit: × 10^4 km^2, statistical significance >99%) from 1952 to 2100, although it also experiences temporary increases in certain years. The simulated near-surface permafrost area decreases from 177.9 × 10^4 km^2 in 1952 to 20.1 × 10^4 km^2 in 2100, with a decreasing rate of 9.9 × 10^4 km^2 per decade.

[28] Active layer thickness simulation and its projection under the A1B emission scenario are given in Figure 5. As shown in Figure 5a, the spatial distribution of the active layer thickness during the period of 1951–1971 can be roughly divided into three subregions: (i) 0.5–1.5 m, located in the center of the permafrost area; (ii) 1.5–2.0 m, located between the center and the edge of the permafrost area; and (iii) 2.0–3.5 m, located at the edge of the permafrost area. During the period from 1951–1971 to 1980–2000, the active layer thicknesses changed relatively little, and the changes occurred primarily at the edge of each subregion. By the period of 2030–2050, the mean active layer thicknesses of 0.5–1.5 m during the period of 1951–1971 increase to 1.5–2.0 m, and the mean active layer thicknesses of 1.5–2.0 m during the period of 1951–1971 increase to 2.0–3.5 m. By the period of 2080–2100, the mean active layer thicknesses of 0.5–1.5 m during the period of 1951–1971 increase significantly to a level of 2.0–3.5 m. Notably, there is a belt (around 34.1°N to 35.04°N; 92.19°E to 100.93°E) where the active layer thickness is relatively shallow and differs distinctly from the near-grid value, although it changes with

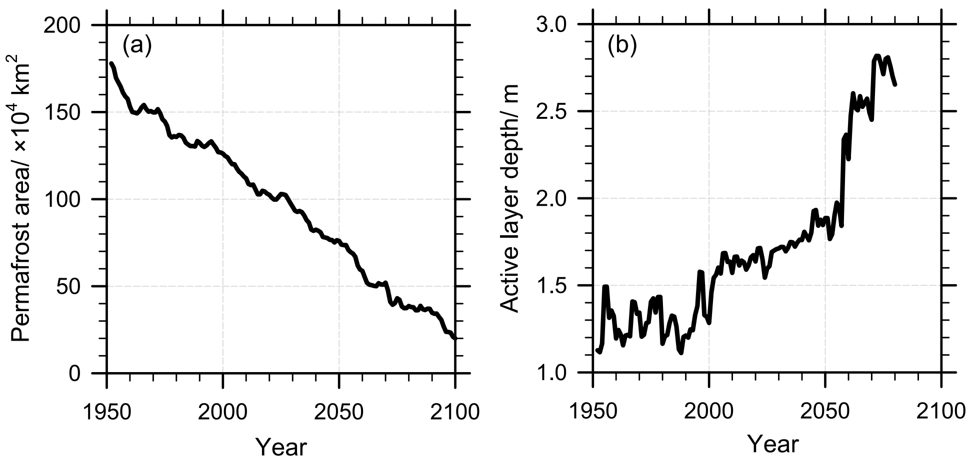

Figure 4. (a) Time series of the simulated near-surface permafrost area (including glaciers and lakes) and (b) the area-mean time series of the simulated active layer depth, as averaged over the permafrost area surrounded by black dashed line in Figure 5d.

time. We find that this is related to the soil organic matter content of those locations where soil organic matter content is significant large and changes slightly with soil depth (figure is not displayed). Possibly, soil organic matter content is inaccurate in those locations because the global organic matter data used in the model are based on relatively few observations. More observations are required to clarify this in the future studies.

[29] Figure 4b shows the area-mean time series of the simulated active layer thickness that is a result averaged over the remaining permafrost area during the period from 2080 to 2100 (the area that is surrounded by the black dashed line in Figure 5d). The active layer thickness exhibits a significantly positive linear trend (y = 0.01x + 0.74, R^2 = 0.84, statistical significance >99%) during the period from 1952 to 2082. Two rapid increases in active layer thickness occur in 2001 and 2057 (detected using the moving t-test technique; a significance level of >99% was used throughout the study). These two rapid increases in active layer thickness are caused by air temperature projected in MIROC/RegCM, which shows coincident rapid increases at years 2001 and 2056 (figure is not displayed). Therefore, the time series

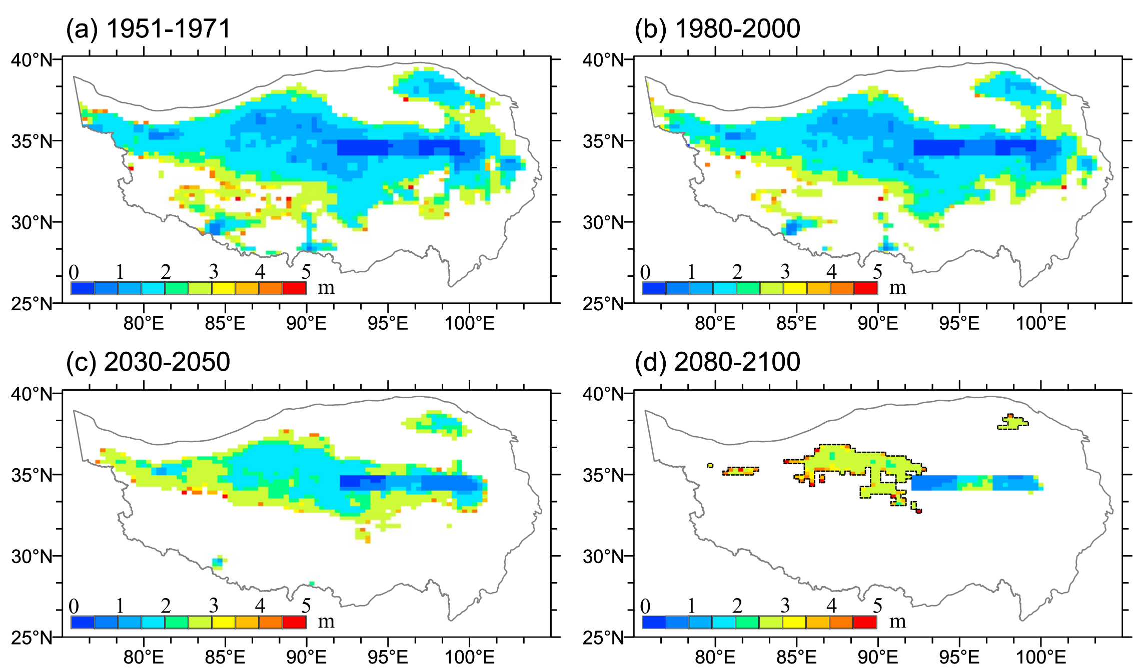

Figure 5. Mean active layer thickness as simulated in the CLM4, as averaged over the period of (a) 1951–1971, (b) 1980–2000, (c) 2030–2050, and (d) 2080–2100. The area surrounded by the black dashed line in Figure 5d is used to calculate the area-mean time series of the simulated active layer depth in Figure 4b.

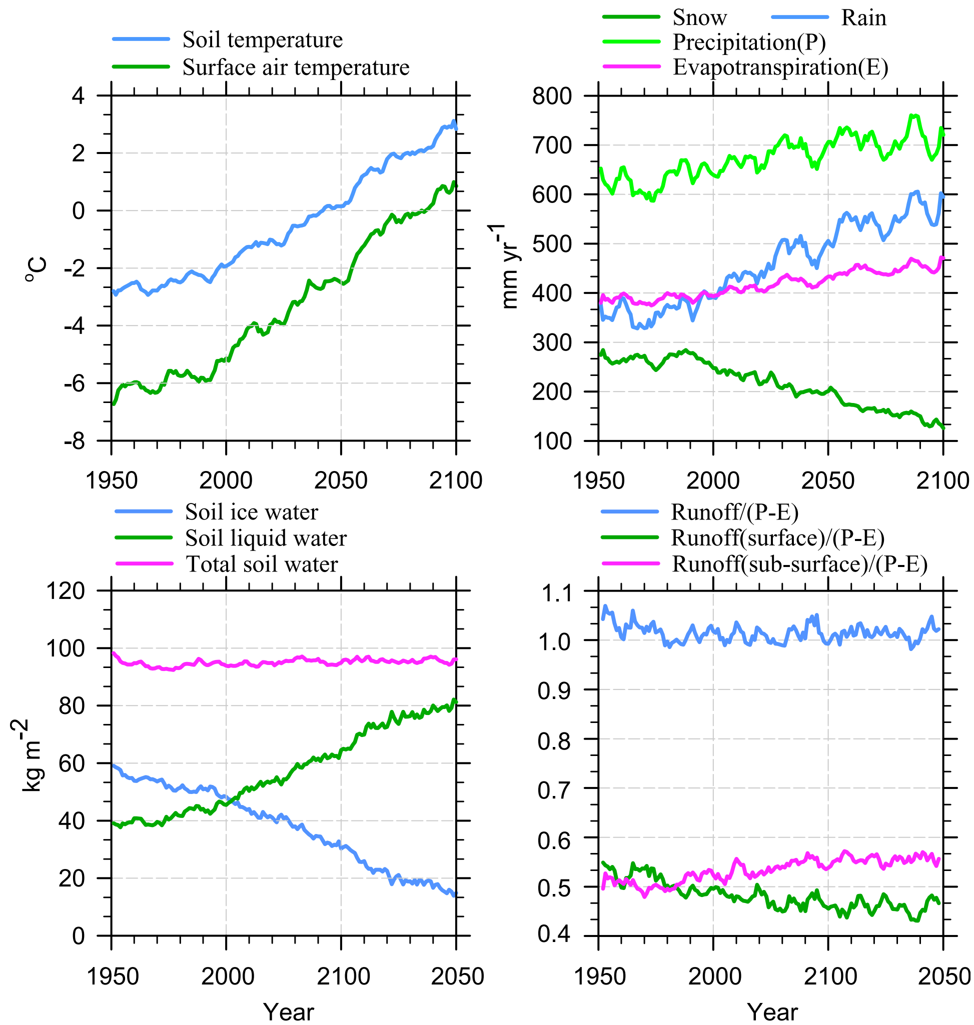

Figure 6. Area-mean time series as averaged over the simulated near-surface permafrost region. Time series are filtered with a 5 year running mean prior to plotting. Soil temperature, ice water, and liquid water are obtained by integrating across all 11 soil levels (0–4.7 m).

of the active layer thickness can be divided into three stages: (i) 1952 to 2001, with an increasing rate of 0.015 m per decade; (ii) 2001 to 2057, with an increasing rate of 0.061 m per decade; and (iii) 2057 to 2082, with an increasing rate of 0.22 m per decade. The relatively high increasing rates during the stage 2057 to 2082 are related to the higher projected air temperature rates during this stage than other stages. It should be noted that these trends are applicable for their averaged area that is located at the northwestern Tibetan Plateau where there is relatively cold permafrost.

3.3. Impact of Permafrost Degradation on Local Hydrological Processes

[30] The area-mean time series of hydrometeorological components for the simulated near-surface permafrost area during the period from 1951 to 1970 is shown in Figure 6. Surface air temperature rises relatively slowly in the 20th century, and this rise accelerates when entering the 21st century. Soil temperature exhibits an increasing trend similar to that of the surface air temperature. Ground ice content begins to decrease as the soil temperature rises, which is especially obvious after entering the 21st century. During the late 21st century, the ground ice content decreases relatively slowly because a small amount of permafrost remains during that time. Owing to the inclusion of the freezing-point depression equation in CLM4, which allows ice to melt over a wide range of temperatures below 0°C, the ground ice content still changes markedly when the soil temperature stays below 0°C. The change in the liquid water content of the soil exhibits an inverse trend to that of the ice content of the soil.

[31] As shown in Figure 6, the levels of rain and snow remain steady in the 20th century; however, when entering the 21st century, rain begins to markedly increase, while snow begins to decrease, which may be related to the increase in air temperature. Evapotranspiration exhibits a relatively weaker and increasing trend, which is due primarily to the increases in total precipitation and in air temperature. Surface runoff decreases relative to the difference between precipitation and evapotranspiration, while subsurface runoff increases at a faster rate than the precipitation-evapotranspiration difference. In addition, total runoff remains steady relative to the

difference between precipitation and evapotranspiration. Ground ice, as a barrier for liquid water to permeate the soil, decreases with permafrost degradation. This results in a larger fraction of liquid water that drains through the soil column more readily and the related reallocation of runoff.

4. Discussion

[32] The physics-based modeling of permafrost is especially difficult in mountainous areas because of the poor representation of rugged and varied topography on coarse grids. The present study projects the permafrost dynamics of the Tibetan Plateau using CLM4, which has a good description of frozen soil processes, forced off-line with high-resolution data from the dynamical downscaling method. The results show that near-surface permafrost degrades severely during the 21st century under the projected Plateau warming. To discuss how plausible this projection is, we compare the results from the previous studies and analyze the potential sources of possible biases in this section.

4.1. Comparison With Previous Research Results

[33] In this work, we provide the total permafrost area for comparison with the permafrost map. If the Tibetan Plateau permafrost is converted into the International Permafrost Association classification system, no continuous permafrost exists on the Tibetan Plateau. Approximately 36.6% of the Plateau permafrost is in the discontinuous zone, 46.6% is in the sporadic zone, and 16.8% is in the isolated patch zone [*Cheng and Wu*, 2007].

[34] Assuming that if the air temperature increases 1°C, the lower limit of the high-altitude permafrost will rise by a certain height in terms of the lapse rate, *Li and Cheng* [1999] used a statistical GIS-aided altitude model to project the future permafrost distribution on the Tibetan Plateau using climatic forcing from the HadCM2 general circulation model scenario of climate change. Their results showed that the Tibetan Plateau permafrost will decrease by 18% as the air temperature rises 1.1°C by 2049, and it will also decrease by 58% as the air temperature rises 2.91°C by 2099 (Table 2). *Nan et al.* [2005] employed a statistical mean annual ground temperature model to project future permafrost distribution on the Tibetan Plateau by considering an air temperature increase of 0.2°C or 0.52°C per decade. In their study, they assumed that the ground temperature and air temperature would increase at the same rate. Their simulation results showed that, in the case of a 0.2°C per decade increase in air temperature, the permafrost area on the Tibetan Plateau will shrink approximately 9% over the next 50 years and 13% over the next 100 years. In the case of a 0.52°C per decade increase in air temperature, the permafrost area on the Tibetan Plateau will shrink by about 14% after 50 years. More remarkable degradation will take place after 100 years, at which point the permafrost area will be reduced by about 46%. When forced off-line with archived data from a fully coupled CCSM3 projection under the SRES A1B, *Lawrence et al.* [2008] used the modified CLM3.5 with a representation of the thermal and hydrologic properties of soil organic matter and a deepening of the soil column to simulate the transient near-surface permafrost evolution north of 45°N during the 21st century. They projected an approximate 88% reduction in near-surface permafrost during the period from 1970–1989 to 2080–2099.

[35] Using CLM4, forced off-line with archived high-resolution data from the RegCM3 nested within the MIROC3.2 HiRes, this work provides a projection of permafrost levels on the Tibetan Plateau under the A1B emission scenario. This emission scenario indicates an area-mean rate of increase of 0.53°C and 0.58°C per decade for the period from 2000 to 2050 and the period from 2000 to 2100, respectively, on the Tibetan Plateau. The air temperature increase is more significant in the northern part of the Plateau during the first half of the 21st century (Figure 7). In terms of the 21st century as a whole, the air temperature increase is more significant in the southwestern and central areas of the Tibetan Plateau (Figure 7). Under the amplitude of the increase in air temperature in this work, the CLM4 projects that the near-surface permafrost area decreases by 39% from the period of 1980–2000 to the period of 2030–2050 and it will also decrease by 81% from the period of 1980–2000 to the period of 2080–2100.

[36] The increase in air temperature on the Tibetan Plateau under the A1B emission scenario is greater than that found in the scenarios used by *Li and Cheng* [1999] and *Nan et al.* [2005]. Importantly, *Li and Cheng* [1999] and *Nan et al.* [2005] used statistical-empirical models with some simple assumptions, while the present study conducted a physics-based modeling of permafrost using a numerical model forced off-line with high-resolution data from a dynamical downscaling method. Despite these differences, the present study predicts more severe permafrost degradation than the studies of *Li and Cheng* [1999] and *Nan et al.* [2005]. In contrast, the present study predicts close but less severe permafrost degradation than the study of *Lawrence et al.* [2008] despite different research regions for both studies.

4.2. How Plausible This Projection Is

[37] In general, one of reasons resulting in the errors in projection of permafrost degradation tends to be the low quality of atmospheric forcing data, especially air temperature. However, a method of dynamical downscaling was used in this study. *Shi* [2010] validated that this dynamical downscaling method yielded a present-day climate more reasonable than the direct output of the global circulation model as compared with the observations in East Asia. Furthermore, air temperature was corrected in this study, which is a climatic factor closely related to permafrost. The corrected temperature fit closely with that of the observations. These indicate that the quality of atmospheric forcing data is relatively high, and this favors the credibility of the projection of permafrost degradation.

[38] One of the other reasons resulting in the errors in projection of permafrost degradation tends to be the poor ability of a land-surface model to simulate permafrost. However, the new version 4 of CLM was used in this study. *Lawrence and Slater* [2005] used the fully coupled CCSM3 with land-surface model CLM3 to examine the transient near-surface permafrost evolution north of 45°N during the 21st century. They predicted a 60% to 90% reduction in the geographic extent of "near-surface permafrost" by 2100. Significant discussion was generated by their results for reasons largely related to the shallow soil profile and the

Table 2. Total Area Containing Frozen Soil (× 10^4 km^2), Calculated Using Different Methods for Selected Periods[a]

Models	Periods	Climatic Warming Rate (°C/Decade)	Permafrost Coverage	Seasonally Frozen Soil and Nonfrozen Soil Coverage
Mean annual ground temperature model [*Nan et al.*, 2005]	Present		120.2	141.7
	50 years later	0.2	109.4 (−9%)	152.6 (+8%)
		0.52	104.0 (−14%)	158.0 (+12%)
	100 years later	0.2	104.1 (−13%)	157.9 (+11%)
		0.52	65.3 (−46%)	196.6 (+39%)
Altitude model [*Li and Cheng*, 1999]	Present		129.4	
	50 years later	0.22	105.6 (−18%)	
	100 years later	0.29	54.1(−58%)	

[a]Figures in parentheses represent the relative change rates in percentages compared with the present-day rates: "−" represents decrease, "+" represents increase.

importance of the organic layer of the surface [e.g., *Burn and Nelson*, 2006; *Lawrence and Slater*, 2006; *Delisle*, 2007; *Yi et al.*, 2007]. Subsequent works focused on the development of CLM3 for the soil temperature simulation and a series of other improvements and addition of new capabilities [*Lawrence et al.*, 2011]. These modifications promoted the release of the CLM4. A brief introduction of the modifications is provided in the section 2 and more detailed information can be found in the literature of *Lawrence et al.* [2011]. *Lawrence et al.* [2008] used the modified version of CLM3.5 to simulate the transient near-surface permafrost evolution north of 45°N during the 21st century again. The model produced a reasonable near-surface permafrost extent compared with that of the observations. The projected severe degradation of permafrost also was basically accepted [*Zimov et al.*, 2006; *Tarnocai et al.*, 2009; *Reyes et al.*, 2010]. Therefore, the CLM4 is applicable for the simulation of permafrost. This also favors the credibility of the projection of permafrost degradation.

[39] Naturally, reasonable air temperature projection is a need for a more credible projection of permafrost degradation. This paper presents an area-mean rate of increase of 0.53°C and 0.58°C per decade for the period from 2000 to 2050 and the period from 2000 to 2100, respectively, on the Tibetan Plateau. *Qin* [2002] projected that air temperatures would increase by a rate of 0.52°C per decade in the next 50 years on the Tibetan Plateau. The increasing rate of 0.53°C per decade of this study is quite close to the value of *Qin* [2002], which indicates that it is a reasonable increasing rate of temperature. In addition, according to the IPCC AR4 under the SRES A1B scenario, the increasing rate of air temperature ranges from 0.28°C to 0.61°C per decade for the period from 2080–2099 to 2080–2099, which is an area-mean result for the Tibetan Plateau [*Meehl et al.*,

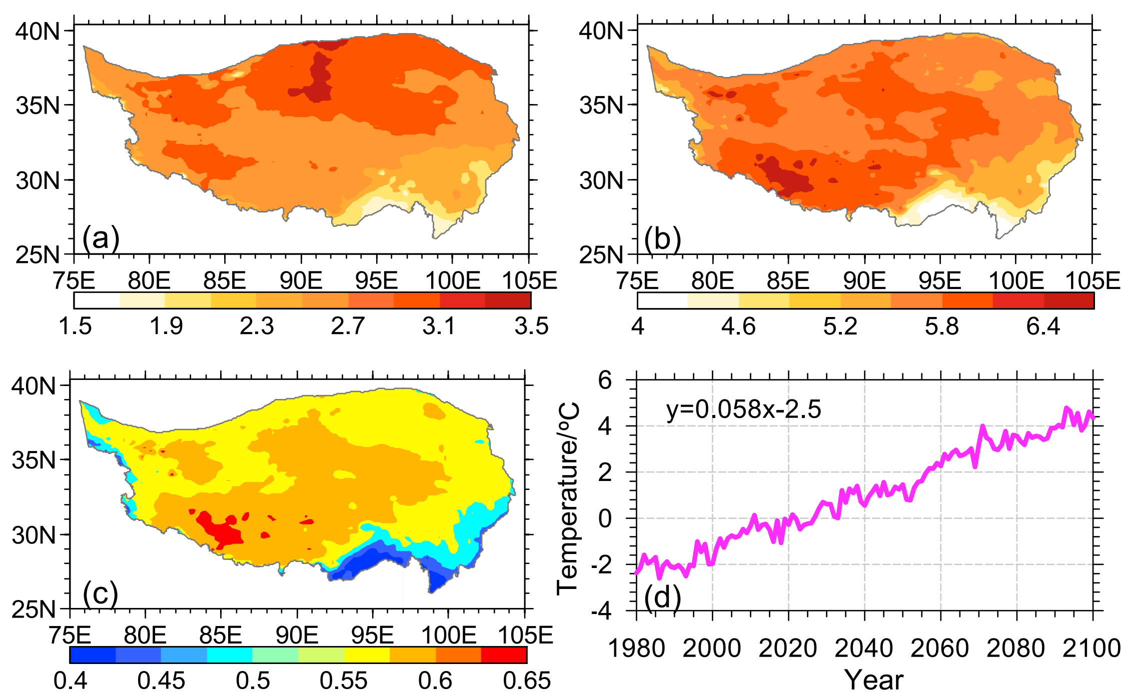

Figure 7. Increase in the surface air temperature (°C) of the forcing data sets (a) between 2030–2049 and 1980–1999 and (b) between 2080–2099 and 1980–1999; (c) trends in the surface air temperature during the period from 1980 to 2100, and (d) the area-mean time series of the surface air temperature, as averaged over the whole Tibetan Plateau.

2007]. Clearly, the increasing rate of this study is within the range of the projection of the IPCC AR4. This also indicates the rationality of the increasing rate of temperature presented in this paper.

[40] The comparison in section 4.1 shows that the present projection of permafrost degradation is larger than that of *Li and Cheng* [1999] and *Nan et al.* [2005]. It is found that these two studies used statistical-empirical models that are incapable of physics-based modeling of permafrost. Furthermore, they stated some simple assumptions. These assumptions may deviate from the reality to some extent. In addition, the increases in air temperature in this paper are larger than those used in these previous studies, though all these increases in temperature are within the reasonable range of the projection for the Tibetan Plateau. Despite different research regions, the present study projects close but less severe permafrost degradation than the study of *Lawrence et al.* [2008], which is based on a similar physics-based modeling of permafrost. These comparative analyses indicate that the present projection may be plausible.

[41] This study performs a physics-based modeling of permafrost based on a relatively high quality of atmospheric forcing data, CLM4 applicable for the simulation of permafrost, and a reasonable air temperature projection. These advantages provide an assurance for the accuracy of projection of the permafrost degradation. However, uncertainties exist in the permafrost simulation. The potential sources of possible uncertainty are discussed in the following section.

4.3. Analysis of Potential Sources of Possible Bias

[42] Regional climate model (RCM)/GCM simulation is difficult on the Tibetan Plateau, and larger differences between the simulated and measured climates exist in this area that are mainly due to the complex topography characteristics [*Gao et al.*, 2008; *Shi*, 2010; *Yu et al.*, 2010]. In this study, we corrected the systematic biases only in the simulated air temperatures, a climatic factor closely related to the permafrost simulation. However, simulated biases in the other forcing elements, e.g., precipitation (snowfall) and radiation, may contribute to some extent to the uncertainty of the permafrost simulation.

[43] The present simulation uses a horizontal resolution of $0.31° \times 0.23°$ in longitude and latitude. This resolution is finer, but the simulation still cannot capture the more detailed regional information for the small-area and isolated permafrost located commonly at the edge of the permafrost boundary; this may contribute to at least part of the bias in the permafrost simulation.

[44] *Lawrence et al.* [2008] demonstrated that experiments with a deep soil column did not exhibit a substantively slower rate of degradation when compared with those with a shallow soil column. They concluded that the 15 layer, approximately 50 m deep, soil column would be sufficient for permafrost change simulations. The CLM4 soil column used in this study was extended to a 15 layer column with a depth of 50 m; thus the soil column depth described in the model could not contribute to the uncertainty in this permafrost simulation.

[45] To some extent, the presence of excess ground ice can retard the rate of permafrost degradation [*Burn and Nelson*, 2006; *Lawrence et al.*, 2008]. *Zhao et al.* [2010] reported that, on average, the permafrost containing excess ground ice occupied approximately 17.8% of the mileage along the Qinghai-Tibetan Highway based on their monitoring of the borehole data set. The present CLM does not explicitly account for excess ground ice, which also results in some of the possible uncertainties in this permafrost simulation.

[46] *Wu et al.* [2010] found that the geothermal gradient within the permafrost layer increases exponentially as the permafrost thickness decreases on the Tibetan Plateau. Permafrost thickness on the Tibetan Plateau ranges from less than 10 to more than 300 m based on direct borehole measurements and indirect estimates calculated by permafrost temperatures at 15 m depth and permafrost temperature gradients. The majority of permafrost on the Tibetan Plateau is less than 100 m in thickness with substantial areas whose permafrost is at a thickness of less than 50 m [*Wu et al.*, 2010]. Such a relatively thin thickness of permafrost means a higher geothermal gradient (or geothermal heat flux) in substantial areas of the Tibetan Plateau. *Wu et al.* [2010] indicated that the geothermal heat flux plays a key role in controlling permafrost temperature and thickness on the Tibetan Plateau. The present CLM also does not explicitly account for geothermal heat flux. It is possible that this is another source of the uncertainty in this permafrost simulation.

[47] It is found that soil organic matter content may be inaccurate and result in the belt of unchanging active layer thickness in Figure 5. Similarly, inaccuracies in the other surface and soil texture data sets employed in this study may also cause the uncertainties in the simulation. In addition, changes in vegetation cover and snow cover can also affect the evolution of soil temperature [*Yang et al.*, 2008; *Lawrence et al.*, 2008]. A dynamic description of the biological processes and an accurate examination of snow cover are required to more reasonably simulate and project the impact of climate change on the permafrost of the Tibetan Plateau.

5. Summary

[48] A projection of permafrost degradation on the Tibetan Plateau during the 21st century under the A1B emission scenario was performed using CLM4 forced off-line with archived high-resolution data from the RegCM3 nested within the MIROC3.2 HiRes. The spatial distribution of simulated permafrost corresponds remarkably well to the frozen soil map, although some detailed information could not be captured because of the relatively large size of the model grid boxes. Simulated permafrost covers a total area of 122.2×10^4 km^2, which compares favorably to the area estimates of 126.7×10^4 km^2 from the frozen soil map.

[49] The mean near-surface permafrost extent clearly decreases by 39% from the period of 1980–2000 to the period of 2030–2050. This degradation occurs primarily at the southern and eastern edges of the simulated permafrost boundary. By the period of 2080–2100, the extent of permafrost decreases by 81% when compared with that of the period of 1980–2000. The simulated near-surface permafrost area exhibits a significant decreasing linear trend from 1952 to 2100, with a rate of decrease of 9.9×10^4 km^2 per decade.

[50] The active layer thickness changed relatively little during the period from 1951–1971 to 1980–2000. By the period of 2030–2050, the active layer thickness of 0.5–1.5 m during the period of 1951–1971 increases to 1.5–2.0 m, and

the active layer thickness of 1.5–2.0 m during the period of 1951–1971 increases to 2.0–3.5 m. By the period of 2080–2100, the active layer thickness of 0.5–1.5 m during the period of 1951–1971 increases significantly to a level of 2.0–3.5 m. The simulated active layer thickness that is averaged over the remaining permafrost area during the period of 2080–2100 exhibits a significant increasing linear trend from 1952 to 2082, with a rate of increase of 0.22 m per decade.

[51] Ground ice content begins to decrease as soil temperature rises, which is especially obvious after entering the 21st century, whereas soil liquid water content exhibits an increasing trend. Surface runoff decreases but subsurface runoff increases, both relative to the difference between precipitation and evapotranspiration. The decrease in ground ice, which is caused by permafrost degradation, allows a larger fraction of liquid water to readily drain through the soil column, resulting in the reallocation of runoff.

[52] The results given in this study indicate the response of permafrost in CLM4 to a certain air temperature increase under the A1B emission scenario. These results may not necessarily reflect actual future permafrost degradation, but they provide a useful reference for the evaluation of the extent of permafrost degradation on the Tibetan Plateau. Further discussion showed that potential sources of possible uncertainty in this permafrost simulation may consist of the simulated biases in the atmospheric forcing elements, the relatively coarse horizontal resolution in the model, the absence of descriptions of excess ground ice and geothermal heat flux in the present CLM4, and inaccuracies in the surface and soil texture data sets employed in this study. A dynamic description of biological processes and an accurate examination of snow cover in the model are required to more reasonably simulate permafrost degradation. Our continued work will be to investigate the amount of permafrost carbon release that results from severe permafrost degradation on the Tibetan Plateau, to use the coupled climate model to examine the response of permafrost to climate change on the Plateau, and to examine the possible feedback of permafrost degradation on the regional or even global climate.

[53] **Acknowledgments.** This research was supported jointly by the National Basic Research Program of China (973 Program) under grant 2009CB421406, the Chinese Academy of Sciences under grants KZCX2-YW-Q1-02 and KZCX2-YW-Q11-05, and the Norwegian Research Council project "East-Asia DecCen." Thanks are due to Xuejie Gao and Ying Shi for providing the atmospheric forcing data set archived from the RegCM3 nested within MIROC3.2 HiRes. Thanks are due to Aihui Wang and Dabang Jiang for helpful discussions regarding the preparation of this paper. We are indebted to three reviewers for helpful comments and criticisms of the initial draft of this paper.

References

Alexeev, V. A., D. J. Nicolsky, V. E. Romanovsky, and D. M. Lawrence (2007), An evaluation of deep soil configurations in the CLM3 for improved representation of permafrost, *Geophys. Res. Lett.*, *34*, L09502, doi:10.1029/2007GL029536.

Anisimov, O. A., and F. E. Nelson (1997), Permafrost zonation and climate change in the northern hemisphere: Results from transient general circulation models, *Clim. Change*, *35*, 241–258, doi:10.1023/A:1005315409698.

Anisimov, O. A., B. Fitzharris, J. O. Hagan, R. Jeffries, H. Marchant, F. E. Nelson, T. Prowse, and D. G. Vaughan (2001), Polar regions (Arctic and Antarctic), in *Climate Change 2001: Impacts, Adaptation, and Vulnerability: Contribution of Working Group II of the Intergovernmental Panel on Climate Change*, edited by J. J. McCarthy et al., pp. 801–841, Cambridge Univ. Press, New York.

Arakawa, A., and W. H. Schubert (1974), Interactions of cumulus cloud ensemble with the large-scale environment. Part I, *J. Atmos. Sci.*, *31*, 674–701, doi:10.1175/1520-0469(1974)031<0674:IOACCE>2.0.CO;2.

Barnett, T. P., L. Dumenil, U. Schlese, E. Roeckner, and M. Latif (1989), The effect of Eurasian snow cover on regional and global climate variations, *J. Atmos. Sci.*, *46*, 661–686, doi:10.1175/1520-0469(1989)046< 0661:TEOESC>2.0.CO;2.

Brown, J., O. Ferrians, J. J. Heginbottom, and E. Melnikov (1997), Circumarctic map of permafrost and ground-ice conditions, scale 1:10,000,000, *U.S. Geol. Surv. Circum-Pac. Map CP-45*.

Burn, C. R., and F. E. Nelson (2006), Comment on "A projection of severe near-surface permafrost degradation during the 21st century" by David M. Lawrence and Andrew G. Slater, *Geophys. Res. Lett.*, *33*, L21503, doi:10.1029/2006GL027077.

Cheng, G. (2002), Interaction between Qinghai-Tibet Railway engineering and permafrost and environmental effects [in Chinese], *Bull. Chin. Acad. Sci.*, *1*, 22–52.

Cheng, G., and T. Wu (2007), Responses of permafrost to climate change and their environmental significance, Qinghai-Tibet Plateau, *J. Geophys. Res.*, *112*, F02S03, doi:10.1029/2006JF000631.

Decker, M. R., and X. Zeng (2009), Impact of modified Richards equation on global soil moisture simulation in the Community Land Model (CLM3.5), *J. Adv. Model. Earth Syst.*, *1*, Art. #5, 22 pp., doi:10.3894/JAMES.2009.1.5.

Delisle, G. (2007), Near-surface permafrost degradation: How severe during the 21st century?, *Geophys. Res. Lett.*, *34*, L09503, doi:10.1029/2007GL029323.

Dickinson, R. E., A. Henderson-Sellers, and P. J. Kennedy (1993), Biosphere Atmosphere Transfer Scheme (BATS) Version 1e as coupled to the NCAR Community Climate Model, NCAR technical note, Nat. Cent. for Atmos. Res., Boulder, Colo.

Emori, S., T. Nozawa, A. Numaguti, and I. Uno (2001), Importance of cumulus parameterization for precipitation simulation over East Asia in June, *J. Meteorol. Soc. Jpn.*, *79*, 939–947, doi:10.2151/jmsj.79.939.

Flanner, M. G., C. S. Zender, J. T. Randerson, and P. J. Rasch (2007), Present-day climate forcing and response from black carbon in snow, *J. Geophys. Res.*, *112*, D11202, doi:10.1029/2006JD008003.

Frauenfeld, O., T. Zhang, and R. Barry (2004), Interdecadal changes in seasonal freeze and thaw depths in Russia, *J. Geophys. Res.*, *109*, D05101, doi:10.1029/2003JD004245.

Fritsch, J. M., and C. F. Chappell (1980), Numerical prediction of convectively driven mesoscale pressure systems. part I: Convective parameterization, *J. Atmos. Sci.*, *37*, 1722–1733.

Fu, X., and D. Zheng (2000), Population growth and sustainable development in the Qinghai–Tibet Plateau [in Chinese], *Resour. Sci.*, *22*, 22–29.

Gao, X., and F. Giorgi (2008), Increased aridity in the Mediterranean region under greenhouse gas forcing estimated from high resolution simulations with a regional climate model, *Global Planet. Change*, *62*, 195–209, doi:10.1016/j.gloplacha.2008.02.002.

Gao, X., Z. Zhao, Y. Ding, R. Huang, and F. Giorgi (2001), Climate change due to greenhouse effects in China as simulated by a regional climate model, *Adv. Atmos. Sci.*, *18*, 1224–1230, doi:10.1007/s00376-001-0036-y.

Gao, X., J. S. Pal, and F. Giorgi (2006), Projected changes in mean and extreme precipitation over the Mediterranean region from a high resolution double nested RCM simulation, *Geophys. Res. Lett.*, *33*, L03706, doi:10.1029/2005GL024954.

Gao, X., Y. Shi, R. Song, F. Giorgi, Y. Wang, and D. Zhang (2008), Reduction of future monsoon precipitation over China: Comparison between a high resolution RCM simulation and the driving GCM, *Meteorol. Atmos. Phys.*, *100*, 73–86, doi:10.1007/s00703-008-0296-5.

Grell, G. (1993), Prognostic evaluation of assumptions used by cumulus parameterizations, *Mon. Weather Rev.*, *121*, 764–787.

Guo, D. L., and H. J. Wang (2012), The significant climate warming in the northern Tibetan Plateau and its possible causes, *Int. J. Climatol.*, doi:10.1002/joc.2388, in press.

Guo, D. L., M. X. Yang, and H. J. Wang (2011a), Characteristics of land surface heat and water exchange under different soil freeze/thaw conditions over the central Tibetan Plateau, *Hydrol. Processes*, *25*, 2531–2541, doi:10.1002/hyp.8025.

Guo, D. L., M. X. Yang, and H. J. Wang (2011b), Sensible and latent heat flux response to diurnal variation in soil surface temperature and moisture under different freeze/thaw soil conditions in the seasonal frozen soil region of the central Tibetan Plateau, *Environ. Earth Sci.*, *63*, 97–107, doi:10.1007/s12665-010-0672-6.

Hasumi, H., and S. Emori (2004), K-1 model developers: K-1 coupled model (MIROC) description, *K-1 Tech. Rep. 1*, Cent. for Clim. Syst.

Res., Univ. of Tokyo, Tokyo, Japan, http://www.ccsr.u-tokyo.ac.jp/kyosei/hasumi/MIROC/tech-repo.pdf.
Holtslag, A., E. de Bruijn, and H. L. Pan (1990), A high resolution air mass transformation model for short-range weather forecasting, *Mon. Weather Rev.*, *118*, 1561–1575, doi:10.1175/1520-0493(1990)118<1561:AHRAMT>2.0.CO;2.
Houghton, J., G. Filho, B. Callander, N. Harris, A. Kattenberg, and K. Maskell (Eds.) (1996), *Climate Change 1995: The Science of Climate Change, Contribution of Working Group I to the Second Assessment Report of the Intergovernmental Panel on Climate Change*, Cambridge Univ. Press, Cambridge, U.K.
Intergovernmental Panel on Climate Change (2000), *Special Report on Emission Scenarios*, edited by N. Nakicenovic et al., 599 pp., Cambridge Univ. Press, New York.
Jones, P. D., and K. R. Briffa (1992), Global surface air temperature variations over the twentieth century: Part 1, spatial, temporal and seasonal details, *Holocene*, *2*, 165–179.
Ju, L. X., H. J. Wang, and D. B. Jiang (2007), Simulation of the Last Glacial Maximum climate over East Asia with a regional climate model nested in a general circulation model, *Palaeogeogr. Palaeoclimatol. Palaeoecol*, *248*, 376–390, doi:10.1016/j.palaeo.2006.12.012.
Lawrence, D. M., and A. G. Slater (2005), A projection of severe near-surface permafrost degradation during the 21st century, *Geophys. Res. Lett.*, *32*, L24401, doi:10.1029/2005GL025080.
Lawrence, D. M., and A. G. Slater (2006), Reply to comment by C. R. Burn and F. E. Nelson on "A projection of near-surface permafrost degradation during the 21st century", *Geophys. Res. Lett.*, *33*, L21504, doi:10.1029/2006GL027955.
Lawrence, D. M., and A. G. Slater (2008), Incorporating organic soil into a global climate model, *Clim. Dyn.*, *30*, 145–160, doi:10.1007/s00382-007-0278-1.
Lawrence, D. M., and A. G. Slater (2010), The contribution of snow condition trends to future ground climate, *Clim. Dyn.*, *34*, 969–981, doi:10.1007/s00382-009-0537-4.
Lawrence, D. M., P. E. Thornton, K. W. Oleson, and G. B. Bonan (2007), Partitioning of evaporation into transpiration, soil evaporation, and canopy evaporation in a GCM: Impacts on land-atmosphere interaction, *J. Hydrometeorol.*, *8*, 862–880, doi:10.1175/JHM596.1.
Lawrence, D. M., A. G. Slater, V. E. Romanovsky, and D. J. Nicolsky (2008), Sensitivity of a model projection of near-surface permafrost degradation to soil column depth and representation of soil organic matter, *J. Geophys. Res.*, *113*, F02011, doi:10.1029/2007JF000883.
Lawrence, D. M., et al. (2011), Parameterization improvements and functional and structural advances in version 4 of the Community Land Model, *J. Adv. Model. Earth Sys.*, *3*, M03001, 27 pp., doi:10.1029/2011MS000045.
Lawrence, P. J., and T. N. Chase (2007), Representing a new MODIS consistent land surface in the Community Land Model (CLM3.0), *J. Geophys. Res.*, *112*, G01023, doi:10.1029/2006JG000168.
Le Treut, H., and Z. X. Li (1991), Sensitivity of an atmospheric general circulation model to prescribed SST changes: Feedback effects associated with the simulation of cloud optical properties, *Clim. Dyn.*, *5*, 175–187.
Li, S., and G. Cheng (1996), Map of permafrost distribution on the Qinghai-Xizang (Tibetan) Plateau [in Chinese], scale 1:3,000,000, Gansu Cultural Press, Lanzhou, China.
Li, X., and G. Cheng (1999), A GIS aided response model of high altitude permafrost to global change, *Sci. China Ser. D*, *42*, 72–79, doi:10.1007/BF02878500.
Liu, J. Y., M. L. Liu, D. F. Zhuang, Z. X. Zhang, and X. Z. Deng (2003), Study on spatial pattern of land-use change in China during 1995–2000, *Sci. China Ser. D*, *46*, 373–384, doi:10.1360/03yd9033.
Lucarini, V., S. Calmanti, A. Dell'Aquila, P. M. Ruti, and A. Speranza (2007), Intercomparison of the northern hemisphere winter mid-latitude atmospheric variability of the IPCC models, *Clim. Dyn.*, *28*, 829–848, doi:10.1007/s00382-006-0213-x.
Manabe, S., and A. Broccoli (1990), Mountains and arid climate of middle latitudes, *Science*, *247*, 192–195, doi:10.1126/science.247.4939.192.
Meehl, G. A., et al. (2007), Global climate projections, in *Climate Change 2007: The Physical Science Basis. Contribution of Working Group I to the Fourth Assessment Report of the Intergovernmental Panel on Climate Change*, edited by S. Solomon et al., pp. 747–845, Cambridge Univ. Press, New York.
Mellor, G. L., and T. Yamada (1982), Development of a turbulence closure model for geostrophic fluid problems, *Rev. Geophys.*, *20*, 851–875, doi:10.1029/RG020i004p00851.
Messerli, B., and J. D. Ives (1997), *Mountains of the World: A Global Priority*, 495 pp., Parthenon, New York.
Muller, S. W. (1947), *Permafrost or Permanently Frozen Ground and Related Engineering Problems*, 231 pp., J. W. Edwards, Ann Arbor, Mich.
Nan, Z., S. Li, and G. Cheng (2005), Prediction of permafrost distribution on Qinghai-Tibet Plateau in the next 50 and 100 years, *Sci. China Ser. D*, *48*, 797–804, doi:10.1360/03yd0258.
Nelson, F. (2003), (Un)frozen in time, *Science*, *299*, 1673–1675, doi:10.1126/science.1081111.
Nelson, F., O. Anisimov, and N. Shiklomanov (2001), Subsidence risk from thawing permafrost, *Nature*, *410*, 889–890, doi:10.1038/35073746.
Nicolsky, D. J., V. E. Romanovsky, V. A. Alexeev, and D. M. Lawrence (2007), Improved modeling of permafrost dynamics in a GCM land-surface scheme, *Geophys. Res. Lett.*, *34*, L08501, doi: 10.1029/2007GL029525.
Niu, G. Y., and Z. L. Yang (2006), Effects of frozen soil on snowmelt runoff and soil water storage at a continental scale, *J. Hydrometeorol.*, *7*, 937–952, doi:10.1175/JHM538.1.
Niu, G. Y., and Z. L. Yang (2007), An observation-based formulation of snow cover fraction and its evaluation over large North American river basins, *J. Geophys. Res.*, *112*, D21101, doi:10.1029/2007JD008674.
Niu, G. Y., Z. L. Yang, R. E. Dickinson, L. E. Gulden, and H. Su (2007), Development of a simple groundwater model for use in climate models and evaluation with Gravity Recovery and Climate Experiment data, *J. Geophys. Res.*, *112*, D07103, doi:10.1029/2006JD007522.
Oelke, C., and T. Zhang (2007), Modeling the active-layer depth over the Tibetan Plateau, *Arct. Antarct. Alp. Res.*, *39*, 714–722, doi:10.1657/1523-0430(06-200)[OELKE]2.0.CO;2.
Oleson, K., et al. (2010), Technical description of version 4.0 of the Community Land Model (CLM), *NCAR Tech. Note NCAR/TN-478+STR*, 266 pp., Natl. Cent. for Atmos. Res., Boulder, Colo.
Pal, J. S., et al. (2007), Regional climate modeling for the developing world: The ICTP RegCM3 and RegCNET, *Bull. Am. Meteorol. Soc.*, *88*, 1395–1409, doi:10.1175/BAMS-88-9-1395.
Pan, D.-M., and D. D. A. Randall (1998), A cumulus parameterization with a prognostic closure, *Q. J. R. Meteorol. Soc.*, *124*, 949–981.
Qin, D. H. (2002), *Evaluation of Environmental Evolvement in West Regions, China (Colligation volume)* [in Chinese], Sci. Press, Beijing.
Reyes, A., D. Froese, and B. Jensen (2010), Permafrost response to last interglacial warming: Field evidence from non-glaciated Yukon and Alaska, *Q. Sci. Rev.*, *29*, 3256–3274, doi:10.1016/j.quascirev.2010.07.013.
Schuur, E., J. Vogel, K. Crummer, H. Lee, J. Sickman, and T. Osterkamp (2009), The effect of permafrost thaw on old carbon release and net carbon exchange from tundra, *Nature*, *459*, 556–559, doi:10.1038/nature08031.
Shi, Y. (2010), A high resolution climate change simulation of the 21st century over East Asia by RegCM3 [in Chinese], PhD dissertation, Inst. of Atmos. Phys., Chin. Acad. of Sci., Beijing.
Shi, Y., X. Gao, Y. Wang, and F. Giorgi (2009), Simulation and projection of monsoon rainfall and rain patterns over eastern China under global warming by RegCM3, *Atmos. Oceanic Sci. Lett.*, *2*, 308–313.
Shi, Y., X. Gao, D. Zhang, and F. Giorgi (2011), Climate change over the Yarlung Zangbo-Brahmaputra River Basin in the 21st century as simulated by a high resolution regional climate model, *Quat. Int.*, *244*, 159–168.
Stendel, M., and J. Christensen (2002), Impact of global warming on permafrost conditions in a coupled GCM, *Geophys. Res. Lett.*, *29*(13), 1632, doi:10.1029/2001GL014345.
Su, Z., T. Zhang, Y. Ma, J. Li, and J. Wen (2006), Energy and water cycle over the Tibetan Plateau: Surface energy balance and turbulent heat fluxes, *Adv. Earth Sci.*, *21*, 1224–1236.
Takata, K., T. Watanabe, and S. Emori (2003), Development of the minimal advanced treatments of surface interaction and runoff, *Global Planet. Change*, *38*, 209–222, doi:10.1016/S0921-8181(03)00030-4.
Tarnocai, C., J. G. Canadell, E. A. G. Schuur, P. Kuhry, G. Mazhitova, and S. Zimov (2009), Soil organic carbon pools in the northern circumpolar permafrost region, *Global Biogeochem. Cycles*, *23*, GB2023, doi:10.1029/2008GB003327.
Thornton, P. E., and N. Zimmerman (2007), An improved canopy integration scheme for a land surface model with prognostic canopy structure, *J. Clim.*, *20*, 3902–3923, doi:10.1175/JCLI4222.1.
Thornton, P. E., J. F. Lamarque, N. A. Rosenbloom, and N. M. Mahowald (2007), Influence of carbon-nitrogen cycle coupling on land model response to CO_2 fertilization and climate variability, *Global Biogeochem. Cycles*, *21*, GB4018, doi:10.1029/2006GB002868.
Thornton, P. E., S. C. Doney, K. Lindsay, J. K. Moore, N. M. Mahowald, J. T. Randerson, I. Fung, J. F. Lamarque, J. J. Feddema, and Y. H. Lee (2009), Carbon-nitrogen interactions regulate climate-carbon cycle feedbacks: Results from an atmosphere-ocean general circulation model, *Biogeosci. Discuss.*, *6*, 3303–3354, doi:10.5194/bgd-6-3303-2009.

Vernekar, A. D., J. Zhou, and J. Shukla (1995), The effect of Eurasian snow cover on the Indian monsoon, *J. Clim.*, *8*, 248–266, doi:10.1175/1520-0442(1995)008<0248:TEOESC>2.0.CO;2.
Wang, A. H., and X. B. Zeng (2009), Improving the treatment of the vertical snow burial fraction over short vegetation in the NCAR CLM3, *Adv. Atmos. Sci.*, *26*(5), 877–886, doi:10.1007/s00376-009-8098-3.
Wang, C., W. Dong, and Z. Wei (2003), Study on relationship between the frozen-thaw process in Qinghai-Xizang Plateau and circulation in East-Asia, *Chin. J. Geophys.*, *46*, 309–316.
Wang, H. J., and J. Q. Sun (2009), Variability of Northeast China river break-up date, *Adv. Atmos. Sci.*, *26*(4), 701–706, doi:10.1007/s00376-009-9035-1.
Wu, Q., and T. Zhang (2008), Recent permafrost warming on the Qinghai-Tibetan Plateau, *J. Geophys. Res.*, *113*, D13108, doi:10.1029/2007JD009539.
Wu, Q., and T. Zhang (2010), Changes in active layer thickness over the Qinghai-Tibetan Plateau from 1995 to 2007, *J. Geophys. Res.*, *115*, D09107, doi:10.1029/2009JD012974.
Wu, Q., T. Zhang, and Y. Liu (2010), Permafrost temperatures and thickness on the Qinghai-Tibet Plateau, *Global Planet. Change*, *72*, 32–38, doi:10.1016/j.gloplacha.2010.03.001.
Wu, T. (2005), A study on response of permafrost to global climate change in Qinghai-Tibetan Plateau [in Chinese], PhD dissertation, Cold and Arid Reg. Environ. and Eng. Res. Inst., Chin. Acad. of Sci., Beijing.
Xu, C., X. Shen, and Y. Xu (2007), An analysis of climate change in east Asia by using the IPCC AR4 simulations [in Chinese], *Adv. Clim. Change Res.*, *3*(5), 287–292.
Xu, Y., X. Gao, Y. Shen, C. Xu, Y. Shi, and F. Giorgi (2009), A daily temperature dataset over China and its application in validating a RCM simulation, *Adv. Atmos. Sci.*, *26*, 763–772, doi:10.1007/s00376-009-9029-z.
Yanai, M., and G. Wu (2006), Effects of the Tibetan Plateau, in *The Asian Monsoon*, edited by B. Wang, pp. 513–549, Springer, New York.
Yanai, M., C. Li, and Z. Song (1992), Seasonal heating of the Tibetan Plateau and its effects on the evolution of the Asian summer monsoon, *J. Meteorol. Soc. Jpn.*, *70*, 319–351.
Yang, M. X., T. D. Yao, and X. H. Gou (2003), The soil moisture distribution, thawing freezing processes and their effects on the seasonal transition on the Qinghai-Xizang (Tibetan) plateau, *J. Asian Earth Sci.*, *21*, 457–465, doi:10.1016/S1367-9120(02)00069-X.
Yang, M. X., T. D. Yao, F. Nelson, N. Shiklomanov, D. L. Guo, and C. Wang (2008), Snow cover and depth of freeze-thaw on the Tibetan Plateau: A case study from 1997 to 1998, *Phys. Geogr.*, *29*, 208–221, doi:10.2747/0272-3646.29.3.208.
Yang, M. X., F. E. Nelson, N. I. Shiklomanov, D. L. Guo, and G. Wan (2010), Permafrost degradation and its environmental effects on the Tibetan Plateau: A review of recent research, *Earth Sci. Rev.*, *103*, 31–44, doi:10.1016/j.earscirev.2010.07.002.
Ye, D., and Y. Gao (1979), *Meteorology of the Tibetan Plateau* [in Chinese], pp. 30–55, Sci. Press, Beijing.
Yi, S., M. K. Woo, and M. A. Arain (2007), Impacts of peat and vegetation on permafrost degradation under climate warming, *Geophys. Res. Lett.*, *34*, L16504, doi:10.1029/2007GL030550.
Yu, E. T., H. J. Wang, and J. Q. Sun (2010), A quick report on a dynamical downscaling simulation over China using the nested model, *Atmos. Ocean. Sci. Lett.*, *3*, 325–329.
Zeng, X. B., and M. Decker (2009), Improving the numerical solution of soil moisture-based Richards equation for land models with a deep or shallow water table, *J. Hydrometeorol.*, *10*, 308–319, doi:10.1175/2008JHM1011.1.
Zeng, X. B., M. Zhao, and R. E. Dickinson (1998), Intercomparison of bulk aerodynamic algorithms for the computation of sea surface fluxes using TOGA COARE and TAO data, *J. Clim.*, *11*, 2628–2644, doi:10.1175/1520-0442(1998)011<2628:IOBAAF>2.0.CO;2.
Zhang, T., R. G. Barry, K. Knowles, J. A. Heginbottom, and J. Brown (1999), Statistics and characteristic of permafrost and ground-ice distribution in the Northern Hemisphere, *Polar Geogr.*, *23*, 132–154, doi:10.1080/10889379909377670.
Zhang, T., F. E. Nelson, and S. Gruber (2007), Introduction to special section: Permafrost and seasonally frozen ground under a changing climate, *J. Geophys. Res.*, *112*, F02S01, doi:10.1029/2007JF000821.
Zhang, Y., W. Chen, and D. Riseborough (2008), Disequilibrium response of permafrost thaw to climate warming in Canada over 1850–2100, *Geophys. Res. Lett.*, *35*, L02502, doi:10.1029/2007GL032117.
Zhao, L. (2004), The freezing-thawing processes of active layer and changes of seasonally frozen ground on the Tibetan Plateau [in Chinese], PhD dissertation, Cold and Arid Reg. Environ. and Eng. Res. Inst., Chin. Acad. of Sci., Beijing.
Zhao, L., Y. Ding, G. Liu, S. Wang, and H. Jin (2010), Estimates of the reserves of ground ice in permafrost regions on the Tibetan Plateau [in Chinese], *J. Glaciol. Geocryol.*, *32*, 1–9.
Zimov, S., E. Schuur, and F. Chapin III (2006), Permafrost and the global carbon budget, *Science*, *312*, 1612–1613, doi:10.1126/science.1128908.

D. Guo and H. Wang, Nansen-Zhu International Research Center, Institute of Atmospheric Physics, Chinese Academy of Sciences, PO Box 9804, Beijing 100029, China. (guodl@mail.iap.ac.cn)

D. Li, National Climate Center, China Meteorological Administration, Beijing 100081, China.